J. Fluid Mech. (2015), *vol.* 781, R4, doi:10.1017/jfm.2015.520

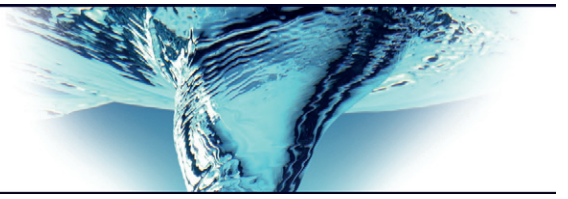

On the distribution and swim pressure of run-and-tumble particles in confinement

Barath Ezhilan[1,‡], **Roberto Alonso-Matilla**[1,‡] **and David Saintillan**[1,†]

[1]Department of Mechanical and Aerospace Engineering, University of California San Diego, 9500 Gilman Drive, La Jolla, CA 92093-0411, USA

(Received 22 July 2015; revised 25 August 2015; accepted 30 August 2015)

The spatial and orientational distribution in a dilute active suspension of non-Brownian run-and-tumble spherical swimmers confined between two planar hard walls is calculated theoretically. Using a kinetic model based on coupled bulk/surface probability density functions, we demonstrate the existence of a concentration wall boundary layer with thickness scaling with the run length, the absence of polarization throughout the bulk of the channel, and the presence of sharp discontinuities in the bulk orientation distribution in the neighbourhood of orientations parallel to the wall in the near-wall region. Our model is also applied to calculate the swim pressure in the system, which approaches the previously proposed ideal-gas behaviour in wide channels but is found to decrease in narrow channels as a result of confinement. Monte Carlo simulations are also performed for validation and show excellent quantitative agreement with our theoretical predictions.

Key words: biological fluid dynamics, micro-organism dynamics, suspensions

1. Introduction

The propensity of confined self-propelled particles to accumulate at boundaries is a trademark of active matter and has been reported in many experiments on bacterial suspensions (Berke *et al.* 2008; Gachelin *et al.* 2013; Figueroa-Morales *et al.* 2015) as well as simulations based on various models (Hernández-Ortiz, Stoltz & Graham 2005; Elgeti & Gompper 2013; Li & Ardekani 2014). Several disparate mechanisms have been proposed in explanation, including wall hydrodynamic interactions (Berke *et al.* 2008) and scattering due to collisions with the walls (Li *et al.* 2011), though recent theoretical efforts have shown that the mere interplay of self-propulsion, stochastic processes and confinement is sufficient to explain accumulation (Lee 2013; Elgeti & Gompper 2015; Ezhilan & Saintillan 2015). With few exceptions, however, these models have necessitated particle diffusion, which in reality is nearly negligible

† Email address for correspondence: dstn@ucsd.edu
‡ These authors contributed equally to this work.

in bacterial suspensions, where stochasticity in the dynamics takes instead the form of run-and-tumble random walks (Berg 1993).

An understanding of the distribution of active particles in confinement is especially critical for determining the mechanical force per unit area exerted by the suspension on the boundaries, or the so-called 'swim pressure'. This novel concept, which has received much scrutiny recently, describes the force that must be applied on containing osmotic walls to keep self-propelled particles confined. Models based on the virial theorem (Takatori, Yan & Brady 2014; Yang, Manning & Marchetti 2014; Winkler, Wysocki & Gompper 2015) and on direct calculations of the wall mechanical pressure (Solon *et al.* 2015*b*) in infinite or semi-infinite collections of spherical swimmers have all arrived at a simple ideal-gas law Π_i for the swim pressure in the limit of infinite dilution:

$$\Pi_i = n\zeta D_t = n\zeta \frac{V_0^2}{3\lambda}, \tag{1.1}$$

where n is the mean number density, ζ is the viscous drag coefficient of a particle and $D_t = V_0^2/3\lambda$ is the long-time translational diffusivity of an unconfined run-and-tumble swimmer expressed in terms of its speed V_0 and mean tumbling rate λ (Berg 1993). Equation (1.1) and its extension to finite concentrations have proven useful to explain motility-induced phase separation in suspensions of self-propelled colloids (Takatori *et al.* 2014; Takatori & Brady 2015), though its general validity as a thermodynamic equation of state for the pressure of active matter remains controversial (Mallory *et al.* 2014; Ray, Reichhardt & Olson Reichhardt 2014; Ginot *et al.* 2015) and appears to be limited to unconfined spherical particles (Yang *et al.* 2014; Solon *et al.* 2015*a*,*b*).

In this work, we analyse the simple case of a dilute suspension of athermal run-and-tumble spherical swimmers confined between two parallel flat plates. We propose in § 2 a kinetic model based on two probability density functions describing the spatial and orientational distribution of the particles inside the gap and at the walls, which are coupled via flux conditions and only account for the effects of swimming and orientation decorrelation by tumbling. Further, our model implicitly captures hard-wall steric interactions without resorting to a soft potential to describe wall collisions as in previous theories (Solon *et al.* 2015*a*,*b*). A semi-analytical solution method is outlined in § 3, which provides the full probability density functions and allows for a direct calculation of the mechanical swim pressure exerted on the walls in terms of the polarization of the surface distributions. Results for the distributions and swim pressure are presented in § 4, where they are shown to compare very favourably with Monte Carlo simulations.

2. Problem definition and theoretical model

2.1. *Problem formulation*

As a minimal model for an active suspension in confinement, we consider a dilute collection of self-propelled spherical particles confined between two infinite parallel plates separated by a distance $2H$ (see figure 1). The swimmers are non-Brownian and simply perform a run-and-tumble random walk: straight runs of duration τ at constant velocity V_0 along the unit director $\boldsymbol{p}$ alternate with instantaneous tumbling events causing random and uncorrelated reorientations of $\boldsymbol{p}$. The time τ between tumbles is an exponentially distributed random variate with mean λ^{-1}, where the tumbling rate λ is assumed to be independent of position and orientation. To elucidate the interplay between run-and-tumble dynamics and confinement, we focus on the dilute limit and entirely neglect interparticle interactions. Particle–wall interactions are purely steric: as

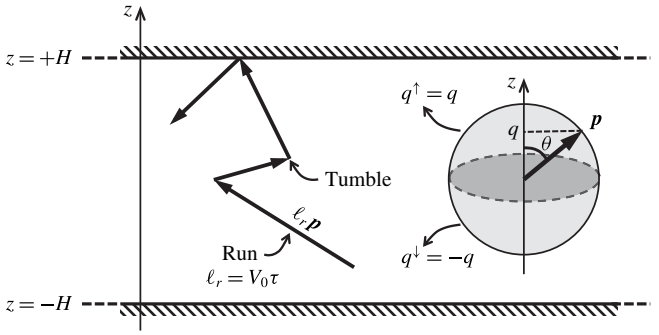

FIGURE 1. Problem definition: run-and-tumble particles are confined between two flat plates separated by $2H$. The distribution of particles is a function of z and $q = \boldsymbol{p} \cdot \hat{\boldsymbol{z}} = \cos\theta \in (-1, 1)$. Orientations pointing towards the top and bottom walls are parametrized by $q^{\uparrow} = q$ and $q^{\downarrow} = -q$ respectively, both defined in $(0, 1)$.

a swimmer meets one of the two surfaces, the normal component of its swimming motion is cancelled by a hard-core repulsive force, causing it to stay at and push against the wall until a subsequent tumbling event reorients it into the bulk. Tumbling events occurring at the walls can lead to reorientation into the wall or into the bulk, so that a particle at a surface may need to undergo more than one tumble before it is able to escape.

There are only two length scales in the problem: the mean run length $\ell_r = V_0\lambda^{-1}$ and the channel width $2H$. We define their ratio as the Péclet number $Pe = \ell_r/2H = V_0/2\lambda H$, where the two limits $Pe \to 0$ and $Pe \to \infty$ describe weak and strong confinement respectively. Due to the symmetry of the problem, the distribution of particles in the channel only depends on two degrees of freedom: the wall-normal coordinate $z \in (-H, H)$ and the wall-normal component of the particle director $q = \boldsymbol{p} \cdot \hat{\boldsymbol{z}} = \cos\theta \in (-1, 1)$. It is convenient to distinguish particles pointing towards the top and bottom walls, and to this end we divide the unit sphere of orientations into two hemispheres and define two distinct orientation coordinates $q^{\uparrow} = q \in (0, 1)$ and $q^{\downarrow} = -q \in (0, 1)$ for particles pointing up or down respectively, as depicted in figure 1.

The distribution of particles in the channel is then fully described by a bulk probability density function $\psi(z, q)$ and two surface probability density functions $\psi_s^{\uparrow}(q^{\uparrow})$ and $\psi_s^{\downarrow}(q^{\downarrow})$, which are only defined over half of the orientations since the surfaces cannot sustain a concentration of particles pointing towards the bulk. By symmetry, we expect

$$\psi(z, -q) = \psi(-z, q), \quad \psi(z, q^{\uparrow}) = \psi(-z, q^{\downarrow}) \quad \text{and} \quad \psi_s^{\uparrow}(q^{\uparrow}) = \psi_s^{\downarrow}(q^{\downarrow}) \qquad (2.1a\text{–}c)$$

for $q^{\uparrow} = q^{\downarrow}$. Next, we describe the coupled bulk/surface conservation equations satisfied by these distributions, together with the appropriate boundary conditions.

2.2. *Bulk conservation equation*

The steady bulk probability density function $\psi(z, q)$ satisfies the conservation equation

$$V_0 q \frac{\partial}{\partial z}\psi(z, q) = -\lambda\psi(z, q) + \frac{1}{2}\int_{-1}^{1} \lambda\psi(z, q')\,\mathrm{d}q'. \qquad (2.2)$$

The left-hand side describes transport along z due to self-propulsion. Run-and-tumble dynamics is captured by the right-hand side, where the first term accounts for depletion due to swimmers tumbling away from orientation q and the second term for restoration due to swimmers tumbling from orientations q' into q. It is also useful to define the orientational moments of order j of the bulk probability density function on the full sphere and on the upper/lower hemispheres of orientations as

$$M_j(z) = \int_{-1}^{1} q^j \psi(z, q)\, \mathrm{d}q \quad \text{and} \quad M_j^{\uparrow\downarrow}(z) = \int_0^1 (q^{\uparrow\downarrow})^j \psi(z, q^{\uparrow\downarrow})\, \mathrm{d}q^{\uparrow\downarrow}, \tag{2.3a,b}$$

and we note that the zeroth, first and second moments correspond to the concentration, polarization and nematic alignment fields:

$$c(z) = M_0(z), \quad m(z) = M_1(z), \quad S(z) = M_2(z), \tag{2.4a–c}$$

$$c^{\uparrow\downarrow}(z) = M_0^{\uparrow\downarrow}(z), \quad m^{\uparrow\downarrow}(z) = M_1^{\uparrow\downarrow}(z), \quad S^{\uparrow\downarrow}(z) = M_2^{\uparrow\downarrow}(z). \tag{2.5a–c}$$

By symmetry, it is straightforward to see that full moments of even order are even functions of z whereas those of odd order are odd functions. With these notations, the bulk conservation equation (2.2) simplifies to

$$\ell_r q \frac{\partial}{\partial z} \psi(z, q) = -\psi(z, q) + \frac{1}{2} c(z). \tag{2.6}$$

Taking the zeroth and first orientational moments of (2.6) and applying symmetry conditions immediately shows that the polarization is zero and the nematic alignment is uniform across the channel:

$$m(z) = 0 \quad \text{and} \quad S(z) = S_0 \quad \forall z \in (-H, H), \tag{2.7a,b}$$

where S_0 is a constant independent of z.

2.3. *Surface conservation equations*

Similarly, conservation equations for the steady surface probability density functions at the walls can be written. We first define the surface concentration and polarization as

$$c_s = \int_0^1 \psi_s^{\uparrow\downarrow}(q^{\uparrow\downarrow})\, \mathrm{d}q^{\uparrow\downarrow} \quad \text{and} \quad m_s = \int_0^1 q^{\uparrow\downarrow} \psi_s^{\uparrow\downarrow}(q^{\uparrow\downarrow})\, \mathrm{d}q^{\uparrow\downarrow}, \tag{2.8a,b}$$

and note that the values of c_s and m_s are the same at both walls. With these notations, the conservation equation at the upper wall ($z = +H$) reads

$$V_0 q^{\uparrow} \psi(H, q^{\uparrow}) = \lambda \left[\psi_s^{\uparrow}(q^{\uparrow}) - \tfrac{1}{2} c_s \right], \tag{2.9}$$

and a similar equation holds at $z = -H$. The right-hand side in (2.9) describes tumbling processes at the wall. The left-hand side, on the other hand, captures the flux of particles that enter the surface from the bulk by self-propulsion, and is therefore proportional to the bulk probability density function $\psi(H, q^{\uparrow})$ next to the wall. Evaluating the zeroth and first moments of (2.9) yields simple relations between c_s and m_s and the values of the bulk moments in the vicinity of the wall:

$$c_s = 2\ell_r m^{\uparrow}(H), \quad m_s - \tfrac{1}{4} c_s = \ell_r S^{\uparrow}(H). \tag{2.10a,b}$$

2.4. *Boundary condition and particle number conservation*

Equation (2.9) can be interpreted as a boundary condition for orientations pointing into the wall. For orientations pointing away from the wall, the swimming flux away from the wall must be balanced by tumbling of particles from the surface towards the bulk. Simply stated, particles on the surface that tumble to an orientation pointing into the bulk are transported away by self-propulsion. This leads to the additional condition

$$V_0 q^{\downarrow}\psi(H, q^{\downarrow}) = \tfrac{1}{2}\lambda c_s \quad \text{or} \quad \ell_r q^{\downarrow}\psi(H, q^{\downarrow}) = \tfrac{1}{2}c_s. \tag{2.11a,b}$$

As c_s is constant and finite, this condition suggests divergence and discontinuity of the bulk probability density function for orientations parallel to the wall ($q^{\downarrow} \to 0$), as will indeed be verified in our analytical solution and stochastic simulations. Taking the zeroth and first moments of (2.11) provides the two additional relations

$$c_s = 2\ell_r m^{\downarrow}(H), \quad c_s = 4\ell_r S^{\downarrow}(H). \tag{2.12a,b}$$

Finally, the above system of equations for the bulk and surface distributions is supplemented by a constraint on the total number of particles in the channel:

$$2c_s + \int_{-H}^{H} c(z)\,\mathrm{d}z = N, \tag{2.13}$$

where N is the particle number in a vertical slice of unit horizontal cross-section.

3. Method of solution and swim pressure calculation

3.1. *Integral equation for the moments*

We now outline a solution method for the system described in § 2. As a first step, we derive an integral equation relating the bulk orientational moments to the concentration field. The bulk concentration equation (2.6) can be viewed as a linear inhomogeneous ordinary differential equation for $\psi(z, q)$, where q is a parameter. We solve it by the method of variation of constants, treating orientations $q^{\uparrow}$ and $q^{\downarrow}$ separately. After applying the boundary condition (2.11), we obtain a general expression for the bulk density function:

$$\psi(z, q^{\uparrow\downarrow}) = \frac{c_s}{2\ell_r q^{\uparrow\downarrow}} \exp\left[-\frac{(H \pm z)}{\ell_r q^{\uparrow\downarrow}}\right] \pm \int_{\mp H}^{z} \frac{c(z')}{2\ell_r q^{\uparrow\downarrow}} \exp\left[\mp\frac{(z - z')}{\ell_r q^{\uparrow\downarrow}}\right] \mathrm{d}z'. \tag{3.1}$$

It should be noted that the bulk and surface concentrations $c(z)$ and c_s both appear on the right-hand side and are still unknown. However, (3.1) shows that their knowledge entirely specifies the bulk distribution $\psi(z, q)$. The bulk moments of order j on both hemispheres of orientations are immediately obtained by integration:

$$M_j^{\uparrow\downarrow}(z) = \frac{c_s}{2\ell_r}\mathscr{E}_{j+1}\left[\frac{H \pm z}{\ell_r}\right] \pm \int_{\mp H}^{z} \frac{c(z')}{2\ell_r}\mathscr{E}_{j+1}\left[\pm\frac{(z - z')}{\ell_r}\right] \mathrm{d}z', \tag{3.2}$$

where $\mathscr{E}_j$ is the exponential integral function defined as

$$\mathscr{E}_j(z) = \int_0^1 u^{j-2} \exp\left(-\frac{z}{u}\right) \mathrm{d}u. \tag{3.3}$$

Finally, the moment of order j on the full sphere of orientations can be shown to be

$$M_j(z) = \frac{c_s}{2\ell_r}\left(\mathscr{E}_{j+1}\left[\frac{H + z}{\ell_r}\right] + \mathscr{E}_{j+1}\left[\frac{H - z}{\ell_r}\right]\right) + \int_{-H}^{H} \frac{c(z')}{2\ell_r}\mathscr{E}_{j+1}\left[\left|\frac{z - z'}{\ell_r}\right|\right] \mathrm{d}z'. \tag{3.4}$$

3.2. *Concentration field and solution procedure*

Setting $j = 0$ in (3.4) immediately provides an integral equation for the yet unknown concentration profile:

$$c(z) = \frac{c_s}{2\ell_r}\left(\mathscr{E}_1\left[\frac{H+z}{\ell_r}\right] + \mathscr{E}_1\left[\frac{H-z}{\ell_r}\right]\right) + \int_{-H}^{H} \frac{c(z')}{2\ell_r}\mathscr{E}_1\left[\left|\frac{z-z'}{\ell_r}\right|\right] \mathrm{d}z'. \tag{3.5}$$

Dividing through by c_s, we obtain an equation for $c(z)/c_s$ that can be solved numerically. For finite ℓ_r, we find that an approximate solution is easily obtained iteratively by casting (3.5) in the form $c_{k+1}(z)/c_s = f[c_k(z)/c_s]$, starting with an initial guess which we take to be $c_0(z) = 0$. In strong confinement ($Pe \gtrsim 10$), the solution converges in $O(20)$ iterations, though more iterations are required in wider channels.

To complete the solution for the concentration field, the value of the surface concentration c_s must be calculated. Having previously obtained $c(z)/c_s$, it is easily evaluated by recasting the constraint (2.13) as

$$c_s = N\left[2 + \int_{-H}^{H} \frac{c(z)}{c_s}\,\mathrm{d}z\right]^{-1}. \tag{3.6}$$

Knowledge of $c(z)$ and c_s then directly provides all of the remaining variables. The bulk probability density function is given by (3.1), while the bulk partial and full moments can be calculated using (3.2) and (3.4). Finally, the surface orientation distribution is provided by (2.9) and the surface polarization by (2.10*b*). Solutions obtained by this method are presented in § 4, where excellent agreement with results from Monte Carlo simulations will be shown.

3.3. *Swim pressure calculation*

The above formulation provides a direct way of estimating the swim pressure in the system, which is simply the force per unit area exerted by the particles at the walls as they push on the surface. Specifically, the normal component of the motion of each particle at the upper wall is resisted by a force $\zeta V_0 q^{\uparrow}$, where ζ is the viscous drag coefficient of one particle (Takatori *et al.* 2014). Knowing the surface probability density function $\psi_s^{\uparrow}$, an expression for the swim pressure is then easily found as

$$\Pi_s = \int_0^1 \zeta V_0 q^{\uparrow}\psi_s^{\uparrow}(q^{\uparrow})\,\mathrm{d}q^{\uparrow} = \zeta V_0 m_s, \tag{3.7}$$

where m_s is the surface polarization. Combining (2.10*b*) and (2.12*b*) to solve for m_s yields a simple relation between the swim pressure and the second moment S_0 of the bulk distribution function:

$$\Pi_s = \zeta V_0 \ell_r[S^{\uparrow}(H) + S^{\downarrow}(H)] = \zeta\frac{V_0^2}{\lambda}S(H) = \zeta\frac{V_0^2}{\lambda}S_0. \tag{3.8}$$

In bulk unconfined systems, previous models have led to the ideal-gas pressure Π_i of (1.1), which contains no information on particle orientations due to isotropy but follows the same scaling as (3.8). To compare the two predictions, we define a dimensionless pressure as the ratio of (3.8) and (1.1):

$$\mathscr{P} = \frac{\Pi_s}{\Pi_i} = \frac{3m_s}{n\ell_r} = \frac{3S_0}{n}, \tag{3.9}$$

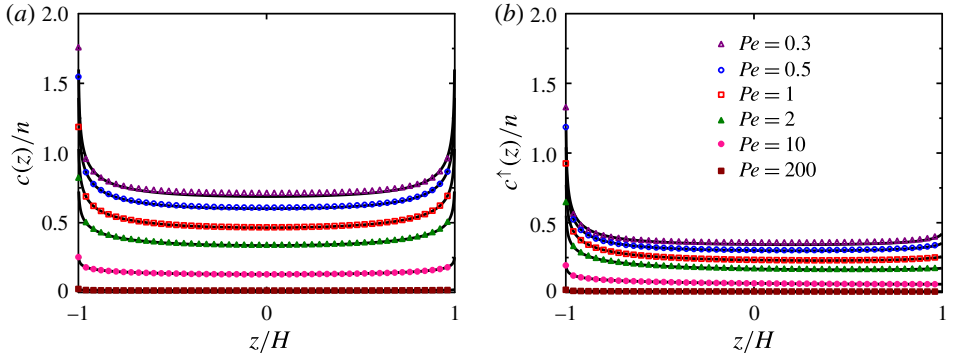

FIGURE 2. Concentration profiles across the channel for various values of $Pe = \ell_r/2H$: (a) full concentration $c(z)$ and (b) partial 'up' concentration $c^{\uparrow}(z)$. The solid lines show the semi-analytical solution of § 3 and the symbols are Monte Carlo simulation results.

where $n = N/2H$ is the mean number density in our system. Here, $\mathscr{P} - 1$ quantifies the departure from the ideal-gas swim pressure. In an infinitely wide channel ($Pe \to 0$), the bulk distribution at the centreline is expected to be isotropic, implying $S_0 = n/3$ and therefore $\mathscr{P} \to 1$. This will be confirmed in our numerical results in § 4, where we also show that $\mathscr{P}$ deviates from 1 when $Pe > 0$ as a result of confinement.

4. Results and comparison with simulations

4.1. *Simulation method*

To validate our model, we also performed Markov-chain Monte Carlo simulations of run-and-tumble swimmers between two hard walls. During a run of duration τ, the swimmer trajectory simply evolves as $\boldsymbol{x}(t + \Delta t) = \boldsymbol{x}(t) + V_0\boldsymbol{p}\Delta t$, where Δt is a short time step. Each run is then followed by a tumbling event, where the new orientation vector $\boldsymbol{p}$ is picked randomly on the unit sphere. The time τ between two consecutive tumbles is drawn from an exponential distribution with cumulative distribution function $F(\tau) = 1 - \exp[-\lambda\tau]$. When a swimmer meets a wall, it remains there and continues to tumble until it reorients towards the bulk and swims away. Time-averaged bulk and surface probability density functions were extracted from orientational and spatial histograms, and convergence was checked with respect to Δt and to the duration of the simulation.

4.2. *Theoretical and numerical results*

Solutions for the bulk concentration profile are depicted in figure 2, where both the full concentration $c(z)$ and the partial 'up' concentration $c^{\uparrow}(z)$ are plotted for various values of the Péclet number, which measures the degree of confinement. The full concentration profiles in figure 2(a) show significant accumulation at the walls, with wall boundary layers whose thickness scales with ℓ_r. An interesting and unique feature of non-interacting and non-aligning spherical run-and-tumble particles is that accumulation occurs in the absence of polarization, and $m(z)$ is found to be strictly zero throughout the channel, as already derived in (2.7). A non-zero polarization would indeed lead to a net flux of particles in the wall-normal direction, which cannot happen in a confined athermal system, unlike in Brownian suspensions where

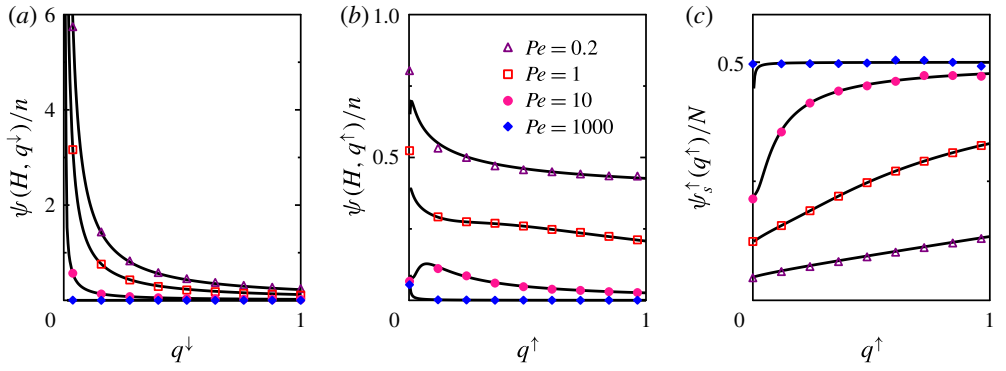

FIGURE 3. Bulk probability density at the top wall for (*a*) orientations pointing away from the wall and (*b*) orientations pointing towards it. (*c*) Surface probability density at the top wall as a function of $q^{\uparrow}$. The solid lines show the semi-analytical solution of § 3 and the symbols are Monte Carlo simulation results.

this flux can be balanced by diffusion (Ezhilan & Saintillan 2015). The profiles also show the presence of a singularity in $c(z)$ at the walls, which is a direct consequence of the boundary condition (2.11) and is also obvious from the solution (3.5) where $\mathscr{E}_1(0)$ diverges. Concentration singularities were also predicted by Elgeti & Gompper (2015), though their model did not capture orientation distributions. As confinement becomes significant and Pe increases, the bulk concentration decreases throughout the channel to reach nearly zero at $Pe = 200$, indicating that strongly confined particles spend most of their time at the boundaries. Excellent quantitative agreement is obtained between theory and Monte Carlo simulations.

Figure 2(*b*) also shows the partial 'up' concentration obtained by only counting particles pointing towards the top wall. The asymmetry of the profiles and the singularity at the bottom wall indicate that on average there are more particles pointing away from the wall than towards it inside the wall accumulation layers. However, in order to satisfy no net polarization in the bulk, this implies that those particles pointing towards the wall are more strongly polarized than those pointing away. This point is confirmed in figure 3(*a*,*b*), showing the orientation distributions in the bulk in the vicinity of the top wall for orientations pointing away from and towards the wall. Figure 3(*a*) confirms the divergence of the bulk probability density in the neighbourhood of orientations parallel to the wall ($q^{\downarrow} \to 0$), as expected from boundary condition (2.11), which is also captured by the simulations. The presence of this discontinuity can be rationalized as follows: particles that leave the surface at an orientation $q^{\downarrow} \gtrsim 0$ swim nearly parallel to the surface and therefore remain there much longer than particles leaving in other orientations. The distribution of particles pointing towards the wall in figure 3(*b*) shows no such singularity, but exhibits a weak finite peak at a critical value of $q^{\uparrow}$ for an intermediate range of Péclet numbers between 5 and 50, whose physical origin remains unclear. The orientation distribution $\psi_s^{\uparrow}(q^{\uparrow})$ of particles on the top wall is shown in figure 3(*c*) and shows a preferential alignment normal to the wall rather than parallel to it. However, this distribution becomes nearly isotropic under very strong confinement ($Pe = 1000$), for reasons that we elucidate below.

Taking moments of $\psi_s^{\uparrow}(q^{\uparrow})$ provides the surface concentration c_s and surface polarization m_s, which are plotted versus the Péclet number in figure 4(*a*,*b*). Both

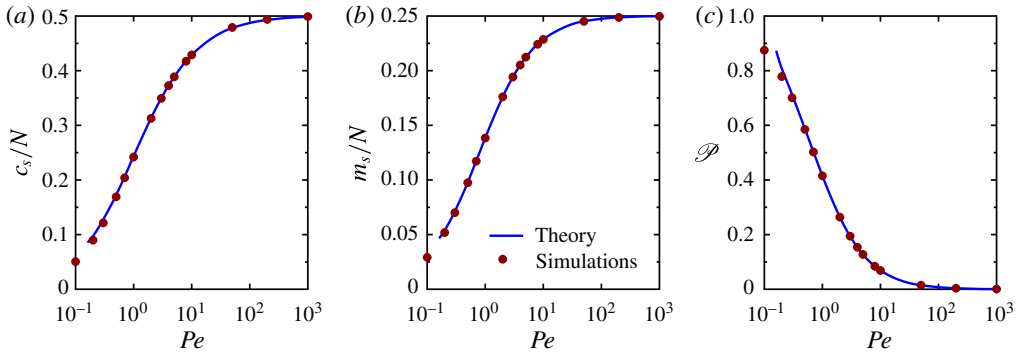

FIGURE 4. (*a*) Surface concentration c_s, (*b*) surface polarization m_s and (*c*) dimensionless pressure $\mathscr{P}$ as functions of the Péclet number $Pe = \ell_r/2H$. The solid lines show the semi-analytical solution of § 3 and the symbols are Monte Carlo simulation results.

quantities increase with increasing confinement, but asymptote as $Pe \to \infty$. The asymptote for c_s is $N/2$, meaning that in very narrow channels the particles spend all of their time at the boundaries; indeed, the time $2H/V_0$ it takes them to cross the gap is infinitesimal compared with the mean run time λ^{-1}. This is also consistent with the decrease in the bulk concentration seen in figure 2(*a*). In this limit, particles tumbling away from one wall reach the other wall nearly instantaneously, leading to an isotropic surface orientation distribution in agreement with figure 3(*c*), hence the asymptote of $N/4$ for the wall polarization.

Lastly, the dependence of the dimensionless swim pressure $\mathscr{P}$ on the degree of confinement is illustrated in figure 4(*c*). In the limit of weak confinement ($H \gg \ell_r$ or $Pe \to 0$), the swim pressure is seen to tend to the ideal-gas law of (1.1) in both our model and simulations: $\mathscr{P} \to 1$ or $\Pi_s \to \Pi_i$. This corresponds to the limit of a single wall where the gap width $2H$ plays no role, and validates the results of previous studies in infinite or semi-infinite systems for which the expression for Π_i was first derived (Takatori *et al.* 2014; Solon *et al.* 2015*b*). Confinement, however, causes a decrease in the swim pressure, which in fact tends to zero for fixed n in very narrow gaps. The high-Pe asymptote for m_s describes the limiting behaviour:

$$\mathscr{P} \to \frac{3}{4} Pe^{-1}, \quad \text{i.e. } \Pi_s \to \frac{3}{4} Pe^{-1} \Pi_i = \frac{nH\zeta V_0}{2} = \frac{N\zeta V_0}{4} \tag{4.1}$$

as $Pe \to \infty$ (or $H \to 0$), which corresponds to $N/2$ particles pushing with an average force of $\zeta V_0/2$ against each wall. The decrease in pressure and the details of the asymptote agree with the previous two-dimensional results of Yang *et al.* (2014), who also verified them in numerical simulations of self-propelled disks. They are also consistent with the study of Ray *et al.* (2014), who analysed the force on two nearby parallel plates in an active particle bath and proposed that the pressure inside the gap in a one-dimensional system with constant run length varies as $\Pi_i/(1 + Pe)$.

4.3. *Summary and discussion*

We have presented a simple continuum model for a dilute suspension of spherical run-and-tumble particles confined between two hard walls and interacting via purely steric forces with the walls. The model improves upon our previous theory for

confined Brownian suspensions (Ezhilan & Saintillan 2015) by allowing us to address the limit of zero temperature within a continuum framework and by incorporating a more realistic treatment of surface interactions and exchange processes between surfaces and the bulk. This description also provides a direct and simple way of calculating the mechanical swim pressure exerted on the walls and serves as a complementary approach to the work of Solon *et al.* (2015*b*), where a continuous description of the same problem using a soft potential for wall interactions was used to calculate the pressure. We have outlined an elegant approach to derive a semi-analytical solution for the probability density functions, and demonstrated excellent quantitative agreement between our model and results from discrete Monte Carlo simulations.

Our theoretical predictions and simulation results have highlighted several striking features of confined suspensions of run-and-tumble particles, namely the presence of a singularity and discontinuity in the bulk probability density function for orientations nearly parallel to the walls in the near-wall region, and the existence of a concentration boundary layer of thickness of the order of ℓ_r that actually diverges at the walls. Our pressure calculations were shown to match the recently proposed ideal-gas equation of state of active matter in wide channels, thus further validating this ideal-gas law and confirming the prediction that the precise nature of particle–wall steric interactions has no impact on the wall mechanical pressure for spherical particles (Solon *et al.* 2015*b*). We demonstrated, however, that confinement leads to departures from this ideal behaviour and specifically to a decrease in the swim pressure, which in fact vanishes in the limit of an infinitely narrow gap when the mean number density is held fixed. In this case, we found that swimmers spend all of their time at the boundaries, which provides the basis for previous models of strongly confined systems that only account for the surface distribution of swimmers (Fily, Baskaran & Hagan 2014).

While capturing the salient features of confined active suspensions, the problem under consideration remained minimal. Yet, the kinetic model presented here could be further modified to incorporate other effects and provide a more realistic description of biological or synthetic active systems. In particular, many active particles are rod-shaped and therefore also incur an aligning torque as they interact with boundaries. Recent theoretical work has shown that the wall pressure is modified in that case and becomes dependent upon the details of particle–wall interactions (Solon *et al.* 2015*a*; Wysocki, Elgeti & Gompper 2015). In addition, experiments show that the surface-to-bulk tumbling of biological swimmers as well as certain types of synthetic swimmers is not uncorrelated but rather results in the preferential release of the particles near a specific angle (Volpe *et al.* 2011; Kantsler *et al.* 2013; Molaie *et al.* 2014). Incorporation of such details in our model is straightforward and would modify the distribution of particles near the walls, with unexpected consequences for the mechanical pressure. Our basic model, validated here in the dilute limit, could also be modified to account for hydrodynamic couplings and to study the structure of the self-generated flows and collective dynamics of interacting active particles in confinement. In more complicated problems such as the ones described above, a complete solution for the bulk and surface probability density functions may not be tractable semi-analytically. Orientational moment equations with a suitable closure model (Saintillan & Shelley 2013; Ezhilan & Saintillan 2015) probably would not perform well either because of the near-wall singularities in the bulk probability density function as well as complications arising from having to develop governing equations and closure approximations for the partial moments as opposed to the full

ones. Extension of the present model to non-planar boundaries, whether concave or convex, is not straightforward either but would be of great interest for the theoretical description of active particle transport in complex geometries or of their interaction with and transport of passive payloads. This rich avenue is the focus of our current work.

Acknowledgements

The authors thank J. F. Brady for seminal discussions and A. Solon for insightful comments. This work was supported by NSF grants CBET-1532652 and DMS-1463965.

References

BERG, H. C. 1993 *Random Walks in Biology*. Princeton University Press.

BERKE, A. P., TURNER, L., BERG, H. C. & LAUGA, E. 2008 Hydrodynamic attraction of swimming microorganisms by surfaces. *Phys. Rev. Lett.* **101**, 038102.

ELGETI, J. & GOMPPER, G. 2013 Wall accumulation of self-propelled spheres. *Europhys. Lett.* **101**, 48003.

ELGETI, J. & GOMPPER, G. 2015 Run-and-tumble dynamics of self-propelled particles in confinement. *Europhys. Lett.* **109**, 58003.

EZHILAN, B. & SAINTILLAN, D. 2015 Transport of a dilute active suspension in pressure-driven channel flow. *J. Fluid Mech.* **777**, 482–522.

FIGUEROA-MORALES, N., MIÑO, G., RIVERA, A., CABALLERO, R., CLÉMENT, E., ALTSHULER, E. & LINDNER, A. 2015 Living on the edge: transfer and traffic of *E. coli* in a confined flow. *Soft Matt.* **11**, 6284–6293.

FILY, Y., BASKARAN, A. & HAGAN, M. F. 2014 Dynamics of self-propelled particles under strong confinement. *Soft Matt.* **10**, 5609–5617.

GACHELIN, J., MIÑO, G., BERTHET, H., LINDNER, A., ROUSSELET, A. & CLÉMENT, E. 2013 Non-Newtonian viscosity of *Escherichia coli* suspensions. *Phys. Rev. Lett.* **110**, 268103.

GINOT, F., THEURFAUFF, I., LEVIS, D., YBERT, C., BOCQUET, L., BERTHIER, L. & COTTIN-BIZONNE, C. 2015 Nonequilibrium equation of state in suspensions of active colloids. *Phys. Rev.* X **5**, 011004.

HERNÁNDEZ-ORTIZ, J. P., STOLTZ, C. G. & GRAHAM, M. D. 2005 Transport and collective dynamics in suspensions of confined swimming particles. *Phys. Rev. Lett.* **95**, 204501.

KANTSLER, V., DUNKEL, J., POLIN, M. & GOLDSTEIN, R. E. 2013 Ciliary contact interactions dominate surface scattering of swimming eukaryotes. *Proc. Natl Acad. Sci. USA* **110**, 1187–1192.

LEE, C. F. 2013 Active particles under confinement: aggregation at the wall and gradient formation inside a channel. *New J. Phys.* **15**, 055007.

LI, G. & ARDEKANI, A. M. 2014 Hydrodynamic interaction of microswimmers near a wall. *Phys. Rev.* E **90**, 013010.

LI, G., BENSSON, J., NISIMOVA, L., MUNGER, D., MAHAUTMR, P., TANG, J. X., MAXEY, M. R. & BRUN, Y. V. 2011 Accumulation of swimming bacteria near a solid surface. *Phys. Rev.* E **84**, 041932.

MALLORY, S. A., SARIĆ, A., VALERIANI, C. & CACCIUTO, A 2014 Anomalous thermomechanical properties of a self-propelled colloidal fluid. *Phys. Rev.* E **89**, 052303.

MOLAIE, M., BARRY, M., STOCKER, R. & SHENG, J. 2014 Failed escape: solid surfaces prevent tumbling of *Escherichia coli*. *Phys. Rev. Lett.* **113**, 068103.

RAY, D., REICHHARDT, C. & OLSON REICHHARDT, C. J. 2014 Casimir effect in active matter systems. *Phys. Rev.* E **90**, 013019.

SAINTILLAN, D. & SHELLEY, M. J. 2013 Active suspensions and their nonlinear models. *C. R. Phys.* **14**, 497–517.

SOLON, A. P., FILY, Y., BASKARAN, A., CATES, M. E., KAFRI, Y., KARDAR, M. & TAILLEUR, J. 2015*a* Pressure is not a state function for generic active fluids. *Nat. Phys.* **11**, 673–678.

SOLON, A. P., STENHAMMAR, J., WITTKOWSKI, R., KARDAR, M., KAFRI, Y., CATES, M. E. & TAILLEUR, J. 2015*b* Pressure and phase equilibria in interacting active Brownian spheres. *Phys. Rev. Lett.* **114**, 198301.

TAKATORI, S. C. & BRADY, J. F. 2015 Towards a thermodynamics of active matter. *Phys. Rev.* E **91**, 032117.

TAKATORI, S. C., YAN, W. & BRADY, J. F. 2014 Swim pressure: stress generation in active matter. *Phys. Rev. Lett.* **113**, 028103.

VOLPE, G., BUTTINONI, I., VOGT, D., KÜMMERER, H.-J. & BECHINGER, C. 2011 Microswimmers in patterned environments. *Soft Matt.* **7**, 8810–8815.

WINKLER, R. G., WYSOCKI, A. & GOMPPER, G. 2015 Virial pressure in systems of active Brownian particles. *Soft Matt.* **11**, 6680–6691.

WYSOCKI, A., ELGETI, J. & GOMPPER, G. 2015 Giant adsorption of microswimmers: duality of shape asymmetry and wall curvature. *Phys. Rev.* E **91**, 050302.

YANG, X., MANNING, M. L. & MARCHETTI, M. C. 2014 Aggregation and segregation of confined active particles. *Soft Matt.* **10**, 6477–6484.